Food Research International 186 (2024) 114320

Contents lists available at ScienceDirect

Food Research International

journal homepage: www.elsevier.com/locate/foodres

Near-infrared spectroscopy to quantify overall thermal process intensity during high-moisture extrusion of soy protein concentrate

Nienke Köllmann [a], Rozemarijn Vringer [a], Puneet Mishra [b], Lu Zhang [a], Atze Jan van der Goot [a,*]

[a] Food Process Engineering, Wageningen University, Bornse Weilanden 9, P.O. Box 17, 6700AA Wageningen, the Netherlands
[b] Wageningen Food and Biobased Research, Bornse Weilanden 9, P.O. Box 17, 6700AA Wageningen, the Netherlands

ARTICLE INFO

Keywords:
Extrusion
Meat analogue
Near-infrared spectroscopy
Process intensity
Shear cell

ABSTRACT

High-moisture extrusion (HME) is widely used to produce meat analogues. During HME the plant-based materials experience thermal and mechanical stresses. It is complicated to separate their effects on the final products because these effects are interrelated. In this study we hypothesize that the intensity of the thermal treatment can explain a large part of the physicochemical changes that occur during extrusion. For this reason, near–infrared (NIR) spectroscopy was used as a novel method to quantify the thermal process intensity during HME. High–temperature shear cell (HTSC) processing was used to create a partial least squares (PLS) regression curve for processing temperature under controlled processing conditions (root mean standard error of cross-validation (RMSECV) = 4.00 °C, coefficient of determination of cross-validation (R^2_{CV}) = 0.97). This PLS regression model was then applied to HME extrudates produced at different screw speeds (200–1200 rpm) and barrel temperatures (100–160 °C) with two different screw profiles to calculate the equivalent shear cell temperature as a measure for thermal process intensity. This equivalent shear cell temperature reflects the effects of changes in local temperature conditions, residence time and thermal stresses. Furthermore, it can be related to the degree of texturization of the extrudates. This information can be used to gain new insights into the effect of various process parameters during HME on the thermal process intensity and extrudate quality.

1. Introduction

High-moisture extrusion (HME) is commonly used to produce fibrous plant-based products with a similar structure to animal meat (Schmid et al., 2022). During this process, plant-based ingredients are mixed with water, sheared, and heated in the extrusion barrel after which the material is pushed through a long cooling die (Opaluwa et al., 2023). Even though extrusion for meat analogue applications was developed already approximately 50 years ago, improvements in the technology seem still possible (Puski & Konwinski, 1976). The development of new extruded products is now mostly based on empirical research, in which the effects of single process parameters on the final product properties are investigated (Emin, 2022). However, the effect of the interactions with other process parameters should be considered as well to better understand the structure formation (Schmid et al., 2022). The hypotheses that are currently available for the mechanisms that cause fibrous structure formation were recently summarized by van der Sman & van der Goot (2023) and Schmid et al. (2022).

One of the prerequisites for fibrous structure formation during HME is the change of physicochemical properties of the ingredients, such as protein denaturation and aggregation or starch gelatinization and degradation (van der Sman & van der Goot, 2023; Z. Zhang et al., 2022). The kinetics of these changes are influenced by the thermal and mechanical treatment of the product inside the extrusion barrel (Pietsch et al., 2019a; Tian et al., 2023). The reactions that take place in the extruder barrel affect the rheological properties and the flow pattern and therefore affect all subsequent steps in the structure formation process (Pietsch et al., 2019b).

Several authors already investigated the effect of ingredient composition (Q. Chen et al., 2023; Nasrollahzadeh et al., 2022; Riazi et al., 2023) or processing conditions (Meng et al., 2022; Sun et al., 2022; X. Zhang et al., 2022) on the changes in protein structure during HME. However, evaluating the effect of all process parameters on the possible reactions for all ingredients used would be extremely time-consuming and costly. Furthermore, the effect of a single process parameter cannot be studied in isolation since they often have interlinked effects on the final products, as is the case for barrel temperature and screw speed (Schmid et al., 2022).

* Corresponding author.
E-mail address: atzejan.vandergoot@wur.nl (A.J. van der Goot).

https://doi.org/10.1016/j.foodres.2024.114320
Received 12 February 2024; Received in revised form 12 April 2024; Accepted 16 April 2024
Available online 18 April 2024

Here, we hypothesize that the thermal treatment is critical to ensure the necessary physicochemical changes in the product and thus the required rheological properties and flow pattern to allow structure formation during HME. This hypothesis relies on the premise that the shear rates the plant-based material experiences during HME are insufficient to initiate protein denaturation (Jaspe & Hagen, 2006), whereas it is well-known that thermal treatment has this effect. This is further supported by the minimum texturization temperature as established by Högg & Rauh (2023), which confirms that thermal treatment is the most important factor for HME structuring. However, it should be noted that shear stresses can lower the activation energy for protein denaturation and affect protein aggregation (Pommet et al., 2004; Quevedo et al., 2020; Sharma & Pandey, 2021; Wolz & Kulozik, 2015). A rapid method to determine the combined effect of multiple extrusion parameters on the thermal process intensity would therefore be desired.

An attempt to develop a rapid method to assess the overall effect of process intensity on extruded pea protein has been already made by Ben-Hdech et al. (1993). They successfully used near-infrared (NIR) spectroscopy in combination with principal component analysis (PCA) to rapidly classify extruded pea protein into different categories based on process intensity. NIR spectroscopy is a rapid and non-destructive measurement technique that relies on the absorption of NIR radiation by CH, OH and NH bonds (Ozaki & Morisawa, 2020). The technique has previously been used to successfully assess the end point temperature of sausages (J. P. Wold et al., 2020), pâté (O'Farrell et al., 2011) and fish products (Skåra et al., 2014; Uddin et al., 2002, 2005, 2006; J. P. Wold, 2016). This applicability of NIR spectroscopy for the measurement of thermal effect mainly relies on the effect of protein denaturation and changes in the protein-water interaction on the NIR spectra (Ellekjaer & Isaksson, 1992; Uddin et al., 2002). NIR measurements of powdered extrudates were previously correlated to the specific mechanical energy input (SME) during cereal extrusion (Guy et al., 1996). However, to the best of our knowledge, NIR has not been applied for the measurement of process intensity of meat analogue products processed by HME yet. This study therefore aims to use NIR spectroscopy to quantify the overall thermal process intensity on products during high-moisture extrusion.

To circumvent the complex interrelated process parameters and high sample amount during HME, high-temperature shear cell (HTSC) processing was used to create a calibration model for thermal process intensity. In this study NIR spectra of HTSC products produced at different processing temperatures were used to create a calibration model for the thermal process intensity using partial least squares (PLS) regression. The influence of processing time (2.5–10 min) on the performance of the calibration model was also quantified, because heating time is known to influence protein denaturation and the NIR spectra of heated protein systems (Skåra et al., 2014). Then, the same calibration model was applied on the NIR spectra of HME extrudates that were produced at different screw speeds (200–1200 rpm), barrel temperatures (100–160 °C) and with two different screw profiles. This method was used to calculate the equivalent shear cell temperature of these extrudates. Subsequently, the effects of these processing parameters on the equivalent shear cell temperature and thus the extent of thermal processing were evaluated. Finally, the relationship between the thermal process intensity and the degree of texturization of the extrudates was explored. This study thus describes a method that quantifies how processing variables influence NIR spectra of HTSC products and extrudates, how these results can be used to generate new insights on the development of inline processing optimisation methods for better quality control of plant-based meat analogues.

2. Materials and methods

2.1. Materials

ALPHA® 8 IP functional soy protein concentrate (SPC) was purchased from Solae, LCC (St. Louis, MO, USA). The dry matter content of the SPC was 93.9 wt% and protein content as measured with the Dumas combustion method 62.0 wt% (Nx5.71) based on dry matter.

2.2. High temperature shear cell processing

To prepare the high-temperature shear cell (HTSC) products, first 39 wt% SPC (on dry matter basis) was manually mixed with demineralized water. The mixture was subsequently hydrated at room temperature for 30 min. The hydrated SPC was then thermo-mechanically treated in an in-house developed HTSC (Grabowska et al., 2016), driven by a Haake PolyLab QC system (Thermo Fisher Scientific, Waltham, MA, USA), at varying conditions. Prior to the thermo-mechanical treatment, the shear cell was pre-heated to the desired processing temperature using an oil bath. After the heat treatment, an additional oil bath was used to cool the product to 50 °C. After complete cooling to room temperature, the products were stored at –20 °C until further usage.

Two different groups of HTSC products were produced by varying processing temperature or time. Firstly, products were produced using a temperature range from 90 to 160 °C with steps of 10 °C at a constant rotational speed of 30 rpm and processing time of 15 min to create the partial least squares (PLS) regression model for processing temperature. Secondly, processing time was varied from 2.5-15 min with steps of 2.5 min at a constant temperature (140 °C) and rotational speed (30 rpm) to evaluate the effect of time on the predicted temperature.

2.3. Extrusion

The extrusion experiments were carried out using a TwinLab-F 20/40 (Brabender GmbH & Co KG, Duisburg, Germany) co-rotating twin screw extruder with a modular cooling die (300 x 25 x 7 mm) (Brabender GmbH & Co KG, Duisburg Germany). The extruder was controlled by MetaBridge software (Brabender GmbH & Co KG, Duisburg, Germany). For all experiments, a screw with a diameter of 20 mm and length-to-diameter ratio of 40 was used. Two different screw profiles (A/B) depicted in Fig. 1 were used. Screw profile A consisted of conveying elements (SE) only. In screw profile B, three types of screw elements were used: SE, a tooth mixing element (Z), and kneading elements (KBW). SE and KBW elements were built in forwarding (R) and reverse directions (L).

The extrusion barrel was divided into four temperature-controlled zones. Each heating zone was heated separately by an electric cartridge heating system and cooled by a water-cooling system (Weinreich WTD 2es, Weinreich Industriekühliung GmbH, Lüdenscheid, Germany). A modular cooling die (300x25x7 mm) was cooled using a refrigerated water circulator set at 25 °C. The extruder responses, including melt temperature, load (%), and pressure were recorded.

The dry powder was fed into the extruder at a feed rate of 4.5 kg/h and the feed moisture content was fixed at 61 wt% (i.e., 39 wt% SPC content). The temperature in the final heating zone (°C) and screw profile were varied according to the experimental design shown in Table 1. For every temperature profile the screw speed was varied from 200-1200 rpm with steps of 200 rpm.

Sample collection was performed when the extruder had reached a constant melt temperature for at least 2 min. The collected samples were stored at −20 °C before further analysis.

2.4. Near-infrared (NIR) measurements

NIR spectral measurements were performed by a Hi-Res, ASD LabSpec spectrometer (Malvern Panalytical, Malvern, United Kingdom). The measurements were performed using an area scan probe (Hi-Brite probe) with a spot size of 10 mm. The probe was placed in a tripod and placed above the sample as close as possible without touching the HTSC product or extrudate. Before measurement the HTSC product or extrudate was completely thawed and the measurement was performed at room temperature. The NIR spectra of the HTSC products were

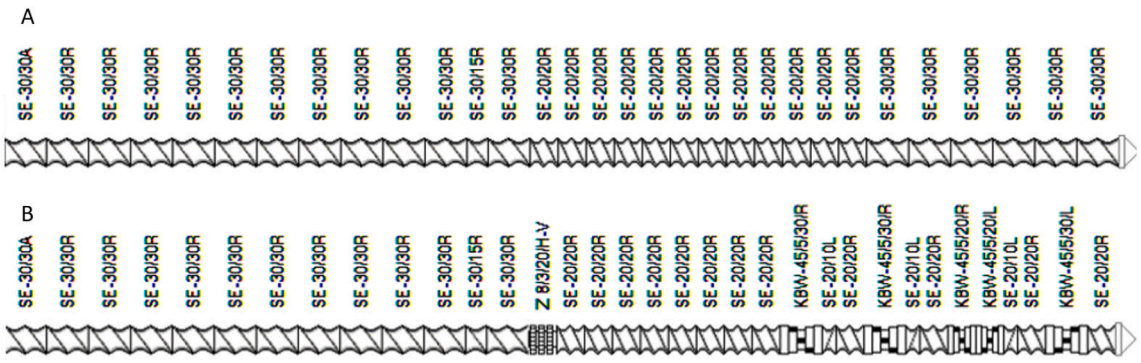

Fig. 1. Overview of the screw profiles used during HME. Screw profile A without kneading or reverse screw elements and screw profile and B with kneading and reverse screw elements.

Table 1
Temperature profiles applied for screw profile A and B during high-moisture extrusion (HME).

Temperature (Heating zone 1|2|3|4 °C)	Screw profile (A/B)
40|80|100|100	A, B
40|80|110|110	B
40|80|110|120	A, B
40|80|110|130	B
40|80|110|140	A, B
40|80|110|150	B
40|80|110|160	A, B

measured in the middle of the HTSC product radius. NIR-spectra of the extrudates were taken at three different locations within one extrusion sample. The probe had an inbuilt 6.5 W halogen light source for illumination and optical fibres were used to capture the reflected light. The instrument was controlled using the Indico Pro software (Malvern Panalytical, Malvern, United Kingdom). The integration time was automatically optimized by the Indico Pro software and was initially set at 15 ms. Each measurement was an average of ~ 5 consecutive measurements automatically performed by the Indico Pro software. The radiometric calibration with white and dark reference was performed by the Indico Pro software automatically.

2.5. NIR data analysis

2.5.1. Pre-processing

NIR spectra in the wavelength range of 400–2200 nm were used for further data analysis. To reduce the effect of colour changes and the high moisture content of our products the use of a reduced wavelength range of 800–1400 nm was also explored. Prior to analysis of the NIR reflectance spectra were transformed to absorbance using a −log transformation. Subsequently, scattering in the NIR reflectance spectra was reduced using standard normal variate (SNV) correction. In SNV correction, each spectrum is centred and divided by its standard deviation, resulting in a common scale for all spectra (Barnes et al., 1989). Finally, the absorbance data was smoothened using the Savitsky-Golay (SAVGOL) (Savitzky & Golay, 1964) algorithm and the 1st derivative was estimated to reveal underlying peaks. A window size of 51 was used for smoothening.

2.5.2. Partial least squares regression

Partial least squares (PLS) regression modelling is a commonly used chemometric technique for the interpretation of NIR spectral data (S. Wold et al., 2001). In this study PLS regression was applied to the HTSC products for which the set heating temperature was the independent variable. Of each processing condition, HTSC experiments of SPC samples were performed in triplicate, yielding three independent HTSC products. NIR spectra of two of these HTSC products were used as calibration set (total of 16 samples), and the third set of samples was served as cross-validation set (total of 8 samples). PLS regression was implemented with MATLAB's default 'plsregress' function (MATLAB R2021b, Natick, WA, USA). A default leave-one-out cross-validation was integrated for optimising the latent variables (LVs). The LVs were then selected by identifying the inflection point. The LV selection results can be found in Fig. S1. PLS regression modelling was performed for both the complete (400–2200 nm) and smaller wavelength range (800–2200 m). The calibration and prediction results were analysed in terms of the root mean standard error of calibration (RMSEC), root mean standard error of the cross-validation (RMSECV), coefficient of determination of calibration (R_c^2), coefficient of determination cross-validation (R_{cv}^2) and prediction bias.

2.5.3. Equivalent shear cell temperature

The PLS regression model for the processing temperature of HTSC products based on the reduced wavelength range of 800–1400 nm was used to calculate the equivalent shear cell temperature from the pre-treated NIR spectra of the extrudates. This equivalent shear cell temperature was used as an indicator of the overall thermal process intensity. It indicates the temperature at which a HTSC product would need to be sheared at 30 rpm for 15 min to achieve a similar thermal process intensity as the extrudate that was measured.

2.5.4. Cutting test for extrudates

The force required for cutting the extrudates was measured using a texture analyser with a load cell of 50 N (TA.XT plusC, Stable Micro Systems, Godalming, Surrey, UK) with a guillotine edge blade (HDP/BS). The thawed extrudates were cut to have approximate size of 24 × 24 mm. Before measurement the texture analyser was set to an initial height of 10 mm. Subsequently, the squared extrudates were compressed to 90 % of its original thickness at a cutting speed of 1 mm/s. The maximum cutting force (*Fmax*) was measured in both parallel and perpendicular direction to the extrusion flow in the cooling die. The degree of texturization was calculated using Eq. (1).

$$Degree\ \ of\ \ texturization = F_{max,\perp} / F_{max,\parallel} \quad (1)$$

In which, $F_{max,\perp}$ is the maximum cutting force in perpendicular direction (N) and $F_{max,\parallel}$ the maximum cutting force in parallel direction (N).

3. Results and discussion

3.1. High-temperature shear cell products

3.1.1. Absorbance spectra

High-temperature shear cell (HTSC) processing was used to study the effect of processing temperature during thermomechanical structuring on the near-infrared (NIR) spectra of the resulting products. Fig. 2 shows

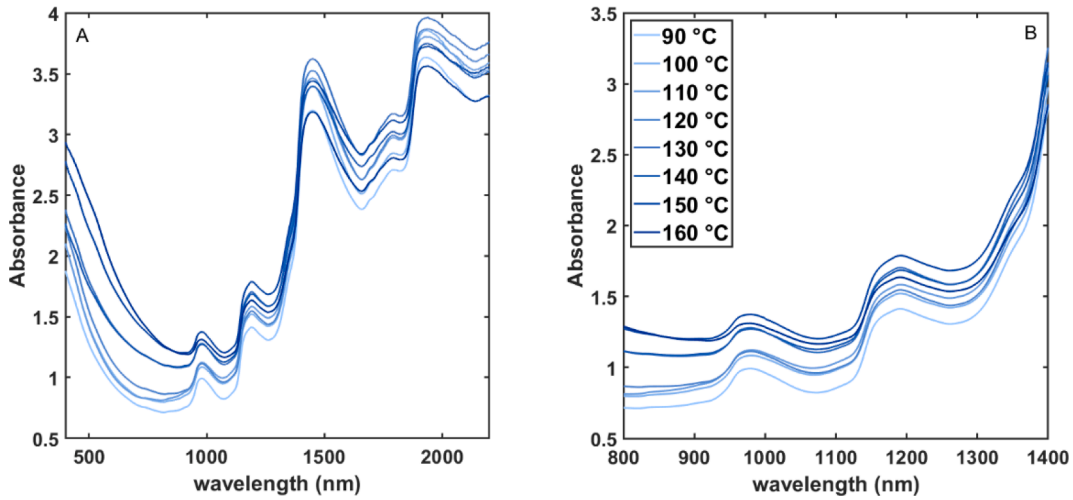

Fig. 2. Absorbance spectra in the full (400–2200 nm) (A) and reduced (800–1400 nm) (B) spectral range of HTSC products treated at temperatures ranging from 90-160 °C, as indicated by colours ranging from light to dark blue, at a constant rotational speed (30 rpm) and processing time (15 min).

the average absorbance spectra in the wavelength ranges of 400–2200 nm and 800–1400 nm of HTSC products that were treated at a temperature ranging from 90-160 °C.

In the visual wavelength range (400–750 nm) the absorbance increases with an increasing processing temperature (Fig. 2A) especially for samples processed at 150 °C and 160 °C. This is in line with the darkened colour of these samples as compared to samples processed at a lower temperature (Fig. S2). The formation of the brown colour could be attributed to Maillard reactions (Taghian Dinani et al., 2023) and/or sugar caramelization (Schmid et al., 2022). Nevertheless, in some previous studies on high-moisture extrusion (HME) and HTSC processing, Maillard reaction products were not detected in obtained products, which could be due to the low amount of reducing sugars in the ingredients used in these studies and the high moisture content that suppresses these reactions (Osen et al., 2015; Wehrmaker et al., 2022).

The main peaks in the absorbance spectra occur around 980, 1200, 1450, and 1930 nm (Fig. 2A). This corresponds with the third overtone of OH, the second overtone of CH, the second overtones of CH, $CONH_2$ and ROH and the first overtone of OH and $CONH_2$ respectively (van Staveren, 2020). These peaks were expected because the products consisted of water, protein, and carbohydrates mainly.

A higher absorbance at around 980 nm was observed when a higher HTSC processing temperature was applied (see Fig. 2A), which suggested an increase in water content of the HTSC products. However, this was not confirmed by measuring the moisture content of the products after processing in the HTSC, expect for products produced at 160 °C, which had a lower moisture content (Fig. S3). Furthermore, an increase in absorbance was not observed in the 1st (1900–1960 nm) and 2nd OH overtone (1400–1450 nm) bands. The higher absorbance at around 980 nm at higher processing temperature can be related to a change in the state of the water or it could be a spectral artefact.

At around 1200 nm, the wavelength corresponding to the 2nd overtone of CH bonds, the absorbance increased with an increasing processing temperature. This indicates that the carbohydrate structure changed due to thermal processing, which was also previously suggested for HME extrudates (De Angelis et al., 2023; Pietsch et al., 2019c).

In addition, we observed an increase of absorbance at 1450 and 1930 nm (which both correlated to $CONH_2$ bonds) when increasing the processing temperature from 90 °C to 130 °C, which indicated the formation of additional peptide bonds and thus protein aggregation. Interestingly, a further increase of the processing temperature from 130 °C to 160 °C led to a decrease in absorbance at 1450 and 1930 nm, indicating a decrease in the number of peptide bonds. We suspect that changing processing temperature of HTSC process influenced protein–protein interactions of soy protein concentrate (SPC) through a complex mechanism: protein aggregation was induced by the heat treatment, while the peptide bonds broken down when the temperature was further increased. This could be due a shift in the balance between disulphide bonds, hydrophobic and electrostatic interactions which all contribute to thermal aggregation (Ju et al., 2023; Liu & Hsieh, 2007). However, Pietsch et al., 2019c and Wittek et al. (2021) did not find a change in protein–protein interactions upon heating during HME at a melt temperature of 100–160 °C or 124/135 °C respectively.

Alternatively, the changes in absorbance at 1930 nm can be attributed to the changes in the carbonyl groups of the protein. Previous research has shown a correlation between the carbonyl groups of whey protein isolate and their NIR spectra because of protein oxidation following thermal treatment (Bordignon et al., 2023). Protein oxidation also occurs during HTSC processing as found by Duque-Estrada et al. (2020) and Wehrmaker et al. (2022). It can therefore be concluded that protein oxidation is one of the physicochemical changes induced by HTSC processing reflected by the NIR absorbance spectra.

To reduce the effect of colour changes and the high water content of our HTSC products on the partial least squares (PLS) regression model for processing temperature, the use of a reduced wavelength range of 800–1400 nm was also explored (Fig. 2B). Thus, the visual wavelength range of 400–750 nm and the strong NIR absorption bands associated with water around 1400–1440 nm and 1900–1950 nm were not included in the PLS regression model (Büning-Pfaue, 2003). The reduced wavelength range resulted in a clearer trend with processing temperature compared to the complete spectra at wider wavelength ranges (Fig. 2). Furthermore, principal component analysis (PCA) analysis showed that the largest part of the variation in these spectra can be related to changes in the processing temperature (Fig. S4).

Summarizing, the effect of temperature on the absorbance spectra indicates that the thermal process intensity indeed affects the protein and carbohydrate properties during the HTSC and HME processes, and that NIR is a suitable technique to capture this effect.

3.1.2. Partial least squares (PLS) regression models

The result of the PLS models based on the complete and reduced wavelength ranges for the processing temperature in the HTSC of products processed at 30 rpm for 15 min are shown in Fig. 3. For both wavelength ranges it was possible to create a PLS model (root mean standard error of calibration (RMSEC) = 1.05 and RMSEC = 3.65) with a low error of cross-validation (root mean standard error of cross-validation (RMSECV) = 4.47 and RMESCV = 4). This indicates that NIR spectroscopy is a suitable technique for the quantification of

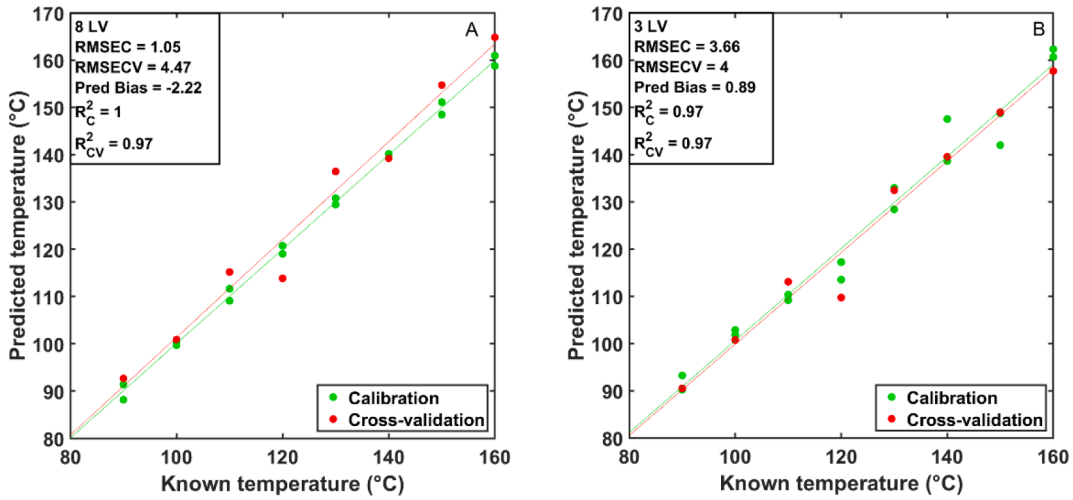

Fig. 3. PLS regression calibration model for processing temperature in the HTSC based on standard normal variate (SNV) + 1st derivative NIR absorbance of the full (400–2200 nm) (A) and reduced (800–1400 nm) (B) spectral range.

thermal effects during HTSC processing. The required number of latent variables (LVs) was higher for the complete spectrum compared to number needed when using the reduced wavelength range. Furthermore, the prediction bias of the model based on the reduced wavelength range was lower (0.89 instead of −2.22). Finally, the difference between the RMSEC and RMSECV was larger for the complete wavelength range compared with the reduced wavelength range which is an indication for overfitting (Shen et al., 2011). For these three reasons the PLS model based on the reduced wavelength range was selected for further analysis of HTSC products and extrudates. This gives an additional advantage being that colour changes and small changes in the water content have a smaller effect on the outcome of the calibration model.

The regression coefficient of the model for the reduced wavelength range is shown in Fig. 4 to better understand which wavelengths and chemical components influence the PLS model for HTSC processing temperature the most. These three wavelengths were 945, 1138 and 1028 nm respectively, as indicated by the high absolute values of the regression coefficient. These wavelengths correspond to the 3rd overtone of OH, the 2nd overtone of CH_3 and 3rd overtone of RNH_2 bonds respectively. Because the main effect of protein denaturation on the NIR spectra is a result of changes in protein confirmation and protein-water interactions, it is not surprising that the overtones related to OH and NH_2 groups contributed most to the regression coefficient. The importance of the 2nd overtone of CH_3 confirms the relevance of the CH bonds for the prediction of processing temperature (De Angelis et al., 2023; Pietsch et al., 2019c). The results described in this section show that NIR spectroscopy is a suitable technique to measure the thermal effect on the different components in plant-based meat analogues.

3.1.3. *Effect of processing time in HTSC on predicted temperature*

Processing time is an important difference between HTSC processing, for which the standard processing time is 15 min, and HME, for which the residence time ranges between 2–5 min (Cornet et al., 2022). Processing time also affects the thermal process intensity, as it influences the extent of protein denaturation, in addition to the heating temperature. Correspondingly, Skåra et al. (2014) reported changes in NIR absorbance of surimi because of both heating temperature and heating time. For this reason, the effect of shorter HTSC processing times (2.5–10 min) on the absorbance spectra and predicted temperature was measured.

The absorbance spectra of the HTSC products produced at shorter processing times showed a similar pattern compared to the HTSC

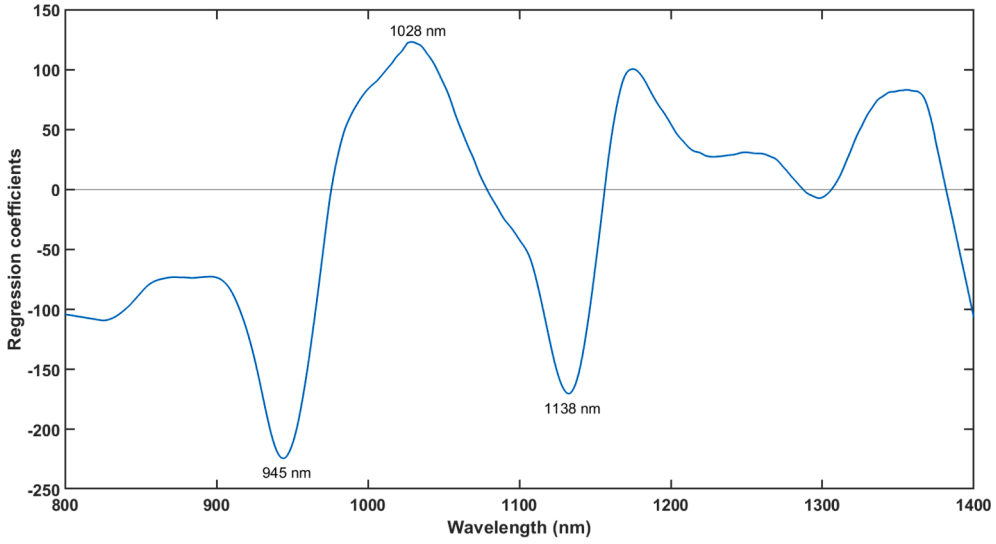

Fig. 4. Regression coefficient PLS regression model for processing temperature in the HTSC based on the reduced (800–1400 nm) spectral range. The highest peaks are annotated with wavelength number.

products on which the PLS regression was based, with peaks around 980 and 1200 nm (Fig. 2 and Fig. 5A). This was expected because the products had the same composition. Nevertheless, the processing time during HTSC processing influenced the absorbance spectra of HTSC products (Fig. 5A). At wavelengths above 1300 nm the absorbance spectra of HTSC products processed for 7.5–15 min were very similar. This indicates that for these processing times the protein-water interactions and protein bonds that are formed are very similar, because this wavelength range is linked to NH and OH overtones (van Staveren, 2020). However, at shorter wavelengths the absorbance increases with increasing processing times from 7.5-15 min.

When applying the PLS regression model for processing temperature it can be observed that shorter processing times resulted in a lower predicted processing temperature (Fig. 5B). The predicted processing temperature stabilizes at processing times $\geq$ 7.5 min, which implicates that physicochemical changes induced by heating mainly occur within the first 7.5 min of the process. This indicates that, to a certain extent, the NIR measurement reflects the time dependency of the reactions that take place during HTSC processing in addition to the effect of temperature and could therefore be used as to quantify the intensity of thermal processing. The typical residence time during HME ranges from 2.5-5 min (Cornet et al., 2022) and residence time is therefore expected to be reflected in the thermal process intensity as measured with NIR spectroscopy with the approach presented in this study.

3.2. Application to extrudates

3.2.1. Absorbance spectra

The average absorbance spectra of extrudates produced with screw profile A (without kneading or reverse screw elements) at 100–160 °C and 200–1200 rpm are shown in Fig. 6. The absorbance spectrum of these HME extrudates shows peaks at similar locations as HTSC products (Fig. 2 and Fig. 6), which was expected given their similar composition. Temperature had a limited effect on the absorbance of these extrudates. However, screw speed resulted in a slight decrease in the absorbance, though this effect is reduced by the applied pre-processing (Fig. S5).

The average absorbance spectra of extrudates produced with screw profile B (with kneading elements) at 100–160 °C and 200–1200 rpm are shown in Fig. 7. These absorbance spectra showed a similar pattern to those of extrudates produced with screw profile A (Fig. 6). However, here, the screw speed affected the NIR spectra of extrudates more. This was not surprising as an increase in screw speed when using screw B will result in a larger increase in the shear stresses and thus in a larger temperature increase caused by viscous dissipation compared to screw profile A (Ellwanger et al., 2023). It should be noted that both an increase in screw speed and temperature resulted in a decreased absorbance, which is opposite to the trend that was observed for the processing temperature for HTSC products (Fig. 2). However, this difference which is most likely caused by baseline shifts is solved by the pre-processing steps applied to the spectra (SNV and 1st derivative) and therefore does not affect the applicability of the PLS regression model (Fig. S6).

It should be noted that pre-processing of the spectral data is crucial for the applicability of the PLS regression model, as it reduces scattering effects caused by structural differences between HTSC products and extrudates. Furthermore, both HTSC and HME products were measured under the same measurement conditions in this study. However, changes in measurement conditions or instrument changes can affect the measured NIR spectra. This should therefore be considered when applying this approach on an industrial scale, for example by standardization of the NIR spectra (J. Zhang et al., 2019).

3.2.2. Equivalent shear cell temperature of extrudates

The calibration curve created for the processing temperature during HTSC processing was applied to the NIR spectra that were measured for the extrudates, to calculate the so-called “equivalent shear cell temperature”. This equivalent shear cell temperature indicates at which processing temperature a product would need to be processed in the HTSC for 15 min at 30 rpm to achieve an equivalent thermal process intensity as during HME. This indicator for thermal processing intensity thus gives insights in the overall process intensity of HME. Thermal process intensity is commonly quantified by the temperature that is measured just before the protein melt enters the cooling die (Ellwanger et al., 2023). For this reason, the equivalent shear cell temperature was plotted versus the measured melt temperature to verify the correlation between these two parameters (Fig. 8).

The equivalent shear cell temperature rose with increasing barrel temperature and screw speed (Fig. 8), which is caused by heating from the barrel wall and viscous dissipation (Mateen et al., 2023). The equivalent shear cell temperature showed a correlation with the measured melt temperature (Table 2). The coefficient of determination of the prediction (R^2_p) when all temperatures were included was higher for screw A ($R^2_p = 0.78$) than screw B ($R^2_p = 0.61$). Moreover, the correlation between the melt temperature and shear cell temperature

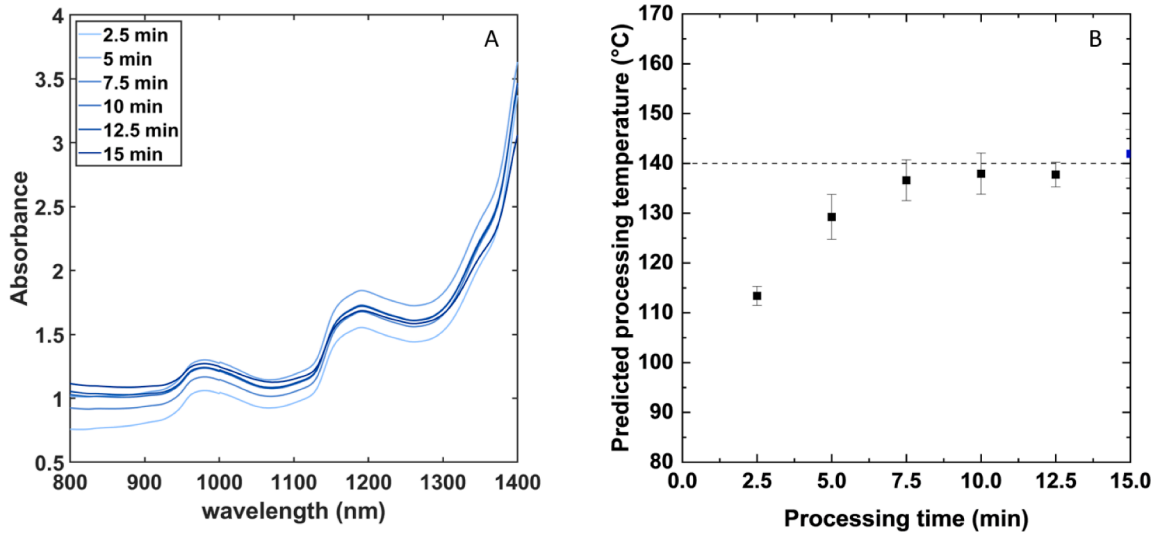

Fig. 5. NIR absorbance spectra of HTSC products produced at varying processing time (A) and the predicted processing temperature of these products (B). Dotted line indicates the set processing temperature. The blue point indicates the processing time that was part of the calibration set of the PLS regression model for processing temperature (15 min).

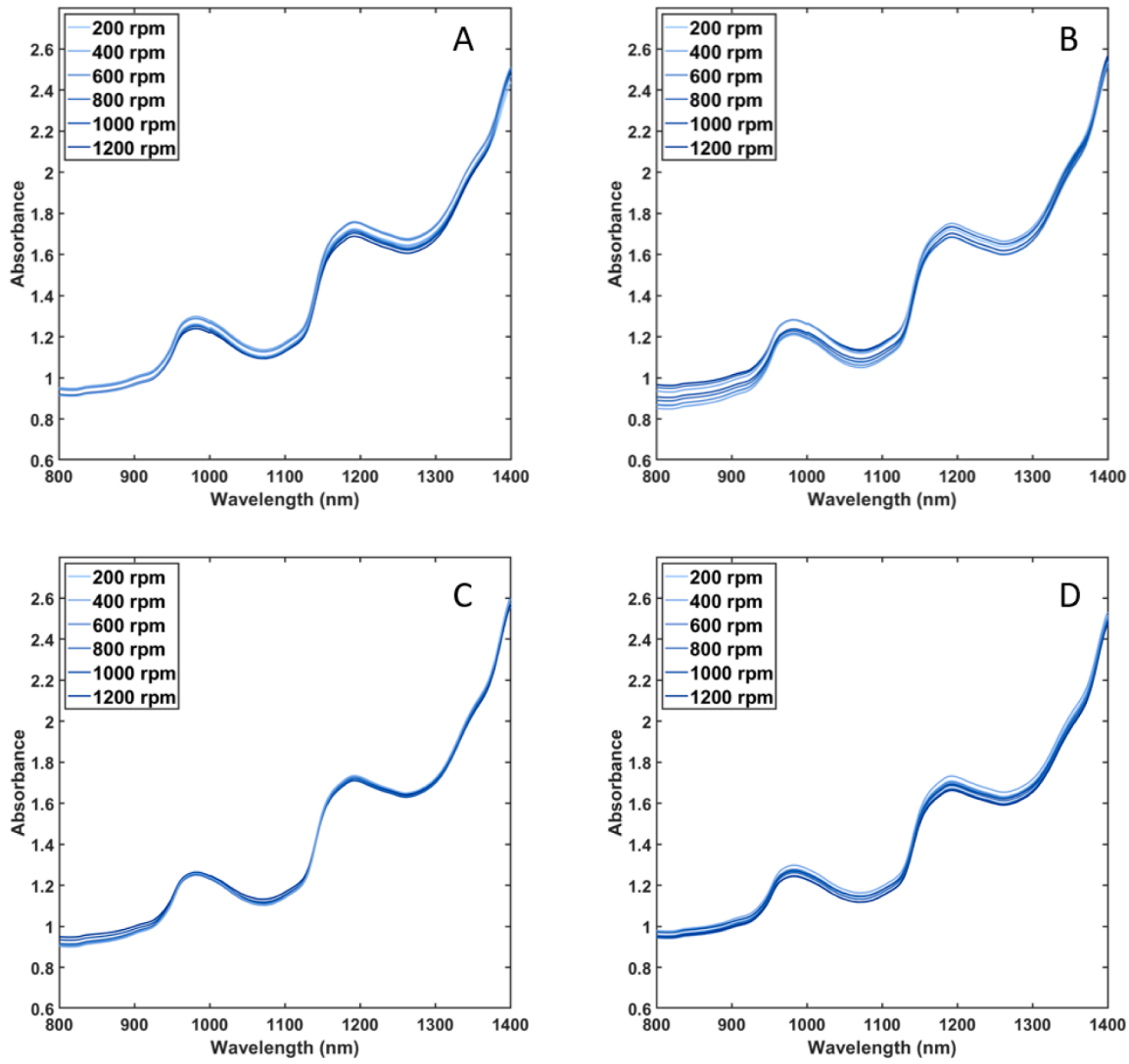

Fig. 6. Absorbance spectra of HME extrudates produced with screw profile A at screw speeds of 200–1200 rpm as indicated by colours ranging from light to dark blue at a barrel temperature of 100 (A), 120 (B), 140 (C) or 160 °C (D).

depended on the barrel temperature that was used and was highest at 100 °C for screw profile A ($R_p^2 = 0.92$) and 130 (R_p^2screwB = 0.82) and 140 °C (R_p^2screwA = 0.85, R_p^2screwB = 0.81) for both screw profiles. Whereas the R_p^2 was lower at barrel temperature > 140 °C. This can be explained by the limited effect of the screw speed on the melt temperature when the barrel temperature is set to ≥ 140 °C, while this is not the case for the equivalent shear cell temperature. This effect is most prominent for screw profile B. A similar influence of barrel temperature on interaction between screw speed and melt temperature was described by Mateen et al. (2023). They showed that a screw speed increase from 300 to 900 rpm had more effect when the barrel temperature wat set to 110 or 130 °C compared with set temperature 150 °C. Pietsch et al., 2019b also observed that screw speed did not significantly contribute to the melt temperature at a barrel temperature of 155 °C, but it did at 100 and 125 °C.

Contrarily to the melt temperature, the equivalent shear cell temperature increased with screw speed at barrel temperatures ≥ 140 °C (Fig. 8). This difference between melt and shear cell temperature is probably caused by the fact that melt temperature only provides information about the thermal process intensity at one position in the process. The shear cell temperature, on the other hand, reflects the total effect of the thermal treatment during HME process and therefore also includes the effect of local temperature maxima. This makes the equivalent shear cell temperature a relevant indicator for overall thermal process intensity, which provides more information than the melt temperature.

Notably, when plotted against melt temperature, the slope of the equivalent temperature increases exponentially with rising barrel temperatures, which is particularly noticeable for extrudates produced at a barrel temperature above 130 °C using screw B. This suggests that mechanical deformation has larger effect on the thermal process intensity than suggested by the melt temperature. This difference can be explained by the influence of local temperature changes resulting from viscous dissipation as was previously described. Additionally, shear stresses could accelerate reactions in the extruder, such as the aggregation and degradation of proteins, as shown for gluten and β–lactoglobulin because shear forces can lower activation energy (Pommet et al., 2004; Quevedo et al., 2020). These changes in chemical properties influence NIR spectra and therefore the equivalent shear cell temperature. However, it should be noted that shear on its own most likely does not cause protein denaturation (Jaspe & Hagen, 2006), but rather reinforces the thermal treatment.

The equivalent shear cell temperature was on average 45 °C lower than the melt temperature for screw A and 30 °C for screw B. The difference between the equivalent shear cell temperature and melt temperature increased with an increase in barrel temperature, which was

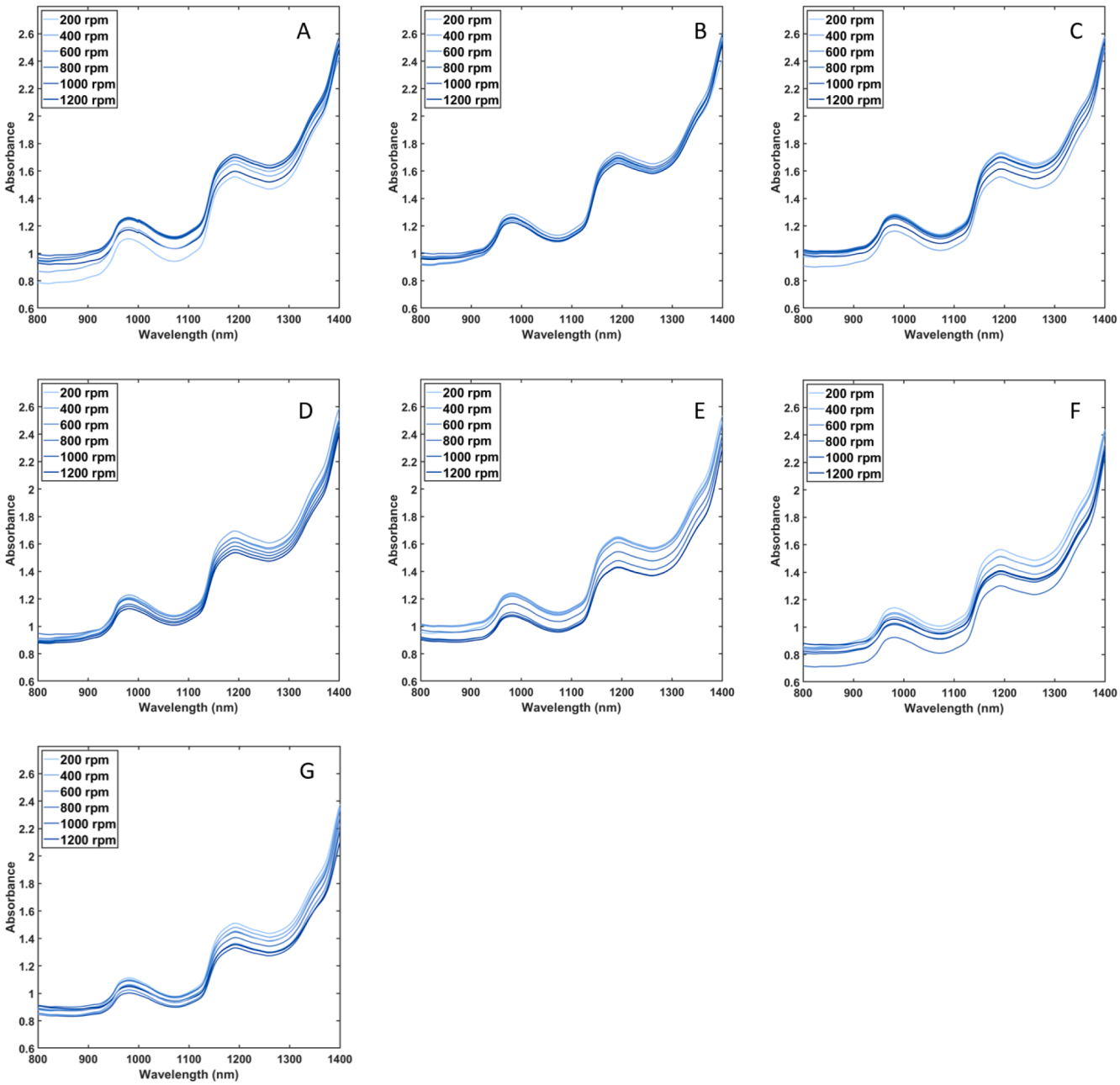

Fig. 7. Absorbance spectra of HME extrudates produced with screw profile B at screw speeds of 200–1200 rpm as indicated by colours ranging from light to dark blue at a barrel temperature of 100 (A), 110 (B), 120 (C), 130 (D), 140 (E), 150 (F) or 160 °C (G).

clearest for screw A. The lower equivalent shear cell T compared to the barrel temperature can probably be attributed to the shorter residence time in the extruder (2–5 min) compared with the HTSC (15 min) (Cornet et al., 2022). This aligns with the effect of processing time on the predicted processing HTSC processing temperature (Fig. 5B). Interestingly, the smaller difference between melt temperature and equivalent shear cell temperature for screw B suggests that the product underwent a more intensive process, probably due longer residence time for extrudates processed with this screw and higher temperature due to viscous dissipation in the kneading zones (Ellwanger et al., 2023). The effect of residence time is not reflected in the melt temperature, which makes the equivalent shear cell temperature a valuable additional parameter for comprehensively studying thermal treatment.

Summarizing, the melt temperature and mechanical deformation influence the equivalent shear cell temperature. Because these parameters both influence the rheological properties of the SPC, they also have an influence on the pressure measured at the die entrance (Pietsch et al., 2019c). This explains why the equivalent shear cell temperature correlates with the barrel pressure (Fig. S7). A schematic overview of the relation between the processing parameters that were varied in this study and the intermediate processes that finally lead to a change in the equivalent shear cell temperature is shown in Fig. 9.

3.2.3. Effect of thermal process intensity on the structural properties of extrudates

The use of the equivalent shear cell temperature as an indicator for thermal process intensity, rather than the melt temperature, may offer an advantage by providing more information on complete effect of thermal processing on the final product properties. To verify this hypothesis the relation between the melt and equivalent shear cell temperature and the degree of texturization of the extrudates produced in this study was explored (Fig. 10). Similar plots for other textural

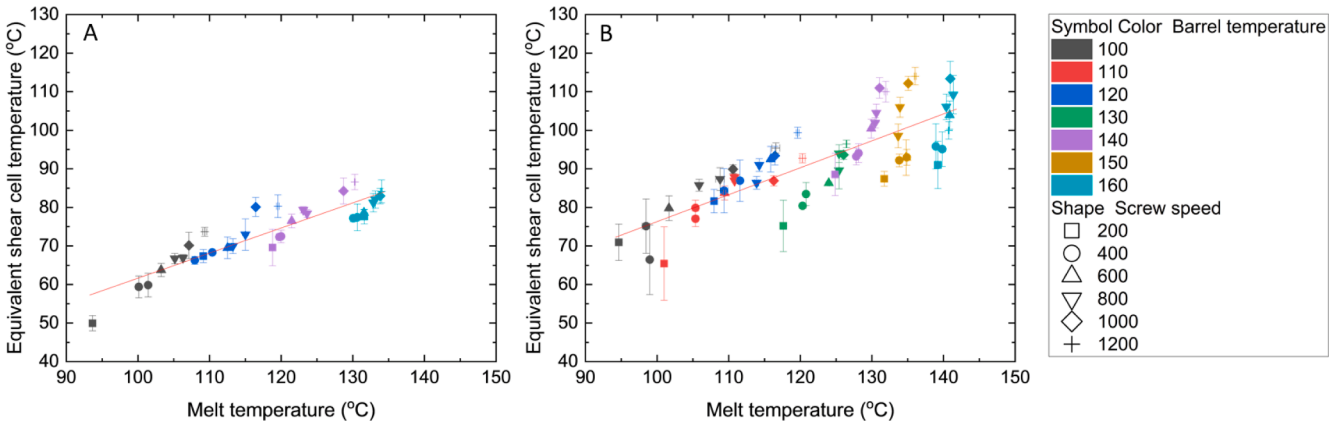

Fig. 8. Equivalent shear cell temperature of extrudates produced with screw profile A (A) and B (B) at 100–160 °C (indicated by symbol colour) and 200–1200 rpm (indicated by symbol shape). Red line is a linear fitted trend line for all data points.

Table 2
Overview residual mean square error of prediction (RMSEP), Prediction bias and R^2p for equivalent shear cell temperature plotted against melt temperature of extrudates.

Barrel temperature	Screw profile A			Screw profile B		
	RMSEP	Bias	R_p^2	RMSEP	Bias	R_p^2
All temperatures	3.92	0.00	0.78	7.25	0.00	0.61
100 °C	1.98	0.00	0.92	5.02	0.00	0.75
110 °C		–		4.55	−0.03	0.71
120 °C	2.67	0.00	0.77	3.14	0.00	0.73
130 °C		–		3.16	0.00	0.82
140 °C	2.28	0.00	0.85	3.48	0.00	0.81
150 °C		–		7.18	0.00	0.44
160 °C	1.95	0.00	0.62	5.41	0.00	0.55

properties (e.g., hardness or cutting strength) can be found in Fig. S8-13. The degree of texturization is calculated as the ratio between the peak cutting force in the perpendicular direction and the parallel direction. A degree of texturization-value larger than 1 indicates alignment, whereas a degree of texturization smaller than 1 indicates an isotropic material without a fibrous or layered structure (Shrestha et al., 2024).

The degree of texturization showed a positive correlation with the melt and shear cell temperature (Fig. 10). Surprisingly, the linear correlation between temperature and degree of texturization was higher for the melt temperature (R^2 = 0.72) than the equivalent shear cell temperature (R^2 = 0.65). When the data of the two screws are split the linear correlation with shear cell temperature for screw A (R^2 = 0.73) was slightly higher than that with the melt temperature (R^2 = 0.76). However, this was not the case for screw B. The increasing effect of temperature on the degree of texturization was previously reported for HME of soy protein isolate (SPI) as well (F. L. Chen et al., 2010; Maung et al., 2021). This effect of temperature on fibrous structure formation can be explained by two effects. Firstly, temperature directly influences the physicochemical changes in of the material in the extrusion barrel (e.g. protein denaturation and aggregation). And secondly, temperature indirectly influences the flow profile in the cooling die, which results from these physicochemical changes (Wittek et al., 2021).

Högg & Rauh (2023) found a minimal texturization temperature of 117.7 °C for HME extrusion of the same type of SPC (Alpha 8) under similar conditions as were used in this study. This is close to the temperature at which the linear trendline for the melt temperature is equal to 1 (119 °C). However, the minimal melt temperature above which all extrudates produced in this study had a texturization index above 1, indicated with the blue dotted line in Fig. 10, is higher (134 °C). It should be noted though that when this temperature is used as target temperature for fibrous structure formation, part of the samples

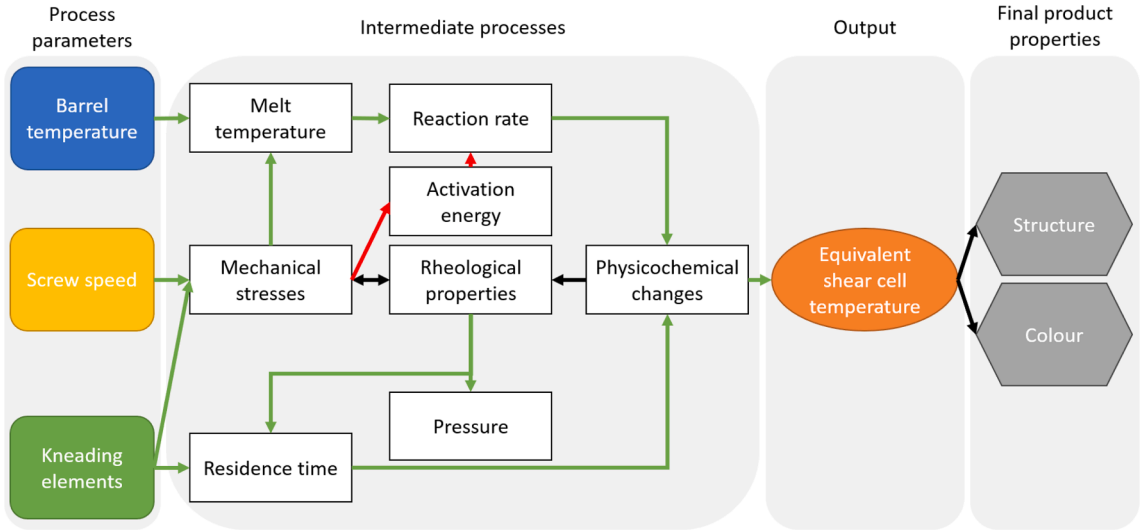

Fig. 9. Schematic overview of the effect of barrel temperature, screw speed and kneading elements on the intermediate processing conditions and the equivalent shear cell temperature. Green arrows indicate a positive relationship, red arrows indicate a negative effect and black arrows effects that can be positive or negative depending on the conditions.

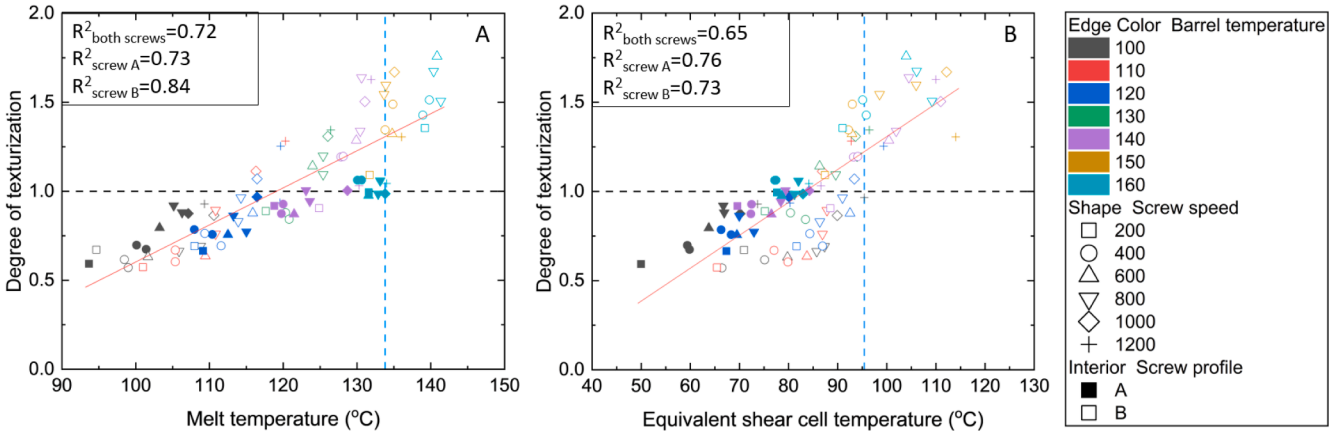

Fig. 10. Degree of texturization of extrudates produced with screw profile A (closed symbols) and B (open symbols) at 100–160 °C (indicated by symbol colour) and 200–1200 rpm (indicated by symbol shape) as measured in cutting test plotted against melt temperature (A) or equivalent shear cell temperature (B). Red line is a linear fitted trend line for all data points. The horizontal black dotted line at a degree of texturization of 1 indicates a structure with isotropic properties. The vertical blue dotted line indicates the temperature above which all extrudates had a degree of texturization above 1.

produced at lower temperature would be rejected unjustified, because these are fibrous. When using the minimal shear cell temperature (95 °C), fewer products were rejected unjustified and a better separation between products with higher and lower texturization indices was achieved. This indicates that the shear cell temperature is more suitable to find the minimal thermal process intensity required for fibrous structure formation than the melt temperature. A likely explanation for this difference is the fact that the equivalent shear cell temperature reflects the overall effect of processing on thermal process intensity, while melt temperature only captures the thermal process intensity just before the die. Thus, shear cell temperature is more representative for the required physicochemical changes.

Fig. 10 shows that extrudates produced with screw A had a higher degree of texturization compared with extrudates produced with screw B at a similar equivalent shear cell temperature. This implies that the physicochemical changes as measured with NIR spectroscopy do not completely explain the structural properties at a larger length scale. However, a degree of texturization slightly above 1 using screw A was only achieved at two processing conditions. A similar trend was observed for the perpendicular cutting strength and other textural properties (hardness, cohesiveness etc.), which indicated stronger products were produced with screw A at temperatures below the minimal temperature for structure formation (Fig. S8-13). We hypothesize that the presence of kneading elements is required to achieve a sufficient thermal process intensity for fibrous structure formation. However, at temperatures below the minimal equivalent shear cell temperature for structure formation, kneading elements can lead to a reduction of the size of the protein aggregates formed in the extruder barrel as was hypothesized by van der Sman & van der Goot (2023). This aggregate size reduction, in turn reduces the degree of texturization, because the cutting force perpendicular to the flow direction decreases (Fig. S9). This effect of the screw configuration indicates that thermal process intensity is not the only factor that determines the structure formation during HME. Interestingly, this effect was only observed when plotting the structural properties against the equivalent shear cell temperature and not the melt temperature. This is an additional indication that the equivalent shear cell temperature provides better insights in the factors influencing fibrous structure formation during HME.

3.2.4. *Future application*

This study demonstrates that NIR in combination with HTSC measurements can be used to get more insight in the processing conditions during HME extrusion of meat analogues. It should be noted though that in this study only a simple formulation consisting of SPC and ~ 61 wt% water was studied. The method can potentially be extended to products that contain more ingredients. To apply this method to these multi-ingredient products, it is necessary to include these formulations in the calibration step and the influence of product homogeneity on the NIR spectra should be considered. This probably means that NIR spectroscopy is interesting for online applications to ensure constant processing conditions during the extrusion process. NIR spectroscopy was already successfully applied online during the extrusion of cereal products (Dodds & Heath, 2005; Evans et al., 1999). Recalibration under processing conditions is required for these in-line measurements. Additionally, the equivalent shear cell temperature is a promising screening tool to find processing conditions that could result in fibrous structures. This is particularly relevant during upscaling from pilot-plant to factory size extruders, as the influence of barrel temperature on the thermal process intensity strongly decreases with larger barrel diameters. In large extruders, heating through viscous dissipation becomes more relevant, while the melt temperature becomes a less accurate measure for the temperature of the product inside the extruder. However, when applying the equivalent shear cell temperature to measure the process intensity of extrudates the NIR measurement conditions of the HTSC products and extrudates should be similar. Finally, NIR spectroscopy can be used as a tool to measure the textural properties of the extrudate in a similar manner as the use of NIR spectroscopy for measurement of the textural properties of animal meat (Schreuders et al., 2021).

4. Conclusion

In this study near-infrared spectroscopy in combination with partial least squares regression was successfully used to create a calibration curve for the processing temperature of high-temperature shear cell (HTSC) products under controlled processing conditions. This model was then used to calculate the equivalent shear cell temperature to assess the thermal process intensity during high-moisture extrusion (HME). The equivalent shear cell temperature reflected the combined effects of shear stresses, (local) temperature effects and the effect of residence time on the thermal process intensity. It was found that the degree of texturization of the extrudates was correlated with the equivalent shear cell temperature. By following a systematic approach this study provides insight into the effect of interrelated processing parameters (e.g., barrel temperature and screw speed) on the thermal process intensity during HME. The knowledge gained could contribute to further optimization of processing conditions to achieve the desired meat analogue products.

CRediT authorship contribution statement

Nienke Köllmann: Writing – review & editing, Writing – original draft, Investigation, Formal analysis, Conceptualization. **Rozemarijn Vringer:** Investigation. **Puneet Mishra:** Writing – review & editing. **Lu Zhang:** Writing – review & editing, Supervision, Conceptualization. **Atze Jan van der Goot:** .

Declaration of competing interest

The authors declare that they have no known competing financial interests or personal relationships that could have appeared to influence the work reported in this paper.

Data availability

Data will be made available on request.

Acknowledgements

The authors would like to thank Imke van der Wee for her contribution to the extrusion trials and texture analysis of the extrudates and Jarno Gieteling for his assistance with the high-temperature shear cell and the extrusion trials.

This research is part of the PlantPromise project, which is co-financed by the Top Consortium for Knowledge and Innovation Agri & Food by the Dutch Ministry of Economic Affairs. The project is registered under contract number LWV-19027.

Appendix A. Supplementary material

Supplementary data to this article can be found online at https://doi.org/10.1016/j.foodres.2024.114320.

References

Barnes, R. J., Dhanoa, M. S., & Lister, S. J. (1989). Standard normal variate transformation and de-trending of near-infrared diffuse reflectance spectra. *Applied Spectroscopy, 43*(5), 772–777. https://doi.org/10.1366/0003702894202201

Ben-Hdech, H., Gallant, D. J., Robert, P., & Gueguen, J. (1993). Use of near infrared spectroscopy to evaluate the intensity of extrusion-cooking processing of pea flour. *International Journal of Food Science & Technology, 28*(1), 1–12. https://doi.org/10.1111/j.1365-2621.1993.tb01246.x

Bordignon, J. C. S., Badaró, A. T., Barbin, D. F., Mariutti, L. R. B., & Netto, F. M. (2023). Oxidation of whey protein isolate after thermal convection and microwave heating and freeze-drying: Correlation among physicochemical and NIR spectroscopy analyses. *Heliyon*, *9*(7), e17981. Doi: 10.1016/J.HELIYON.2023.E17981Büning-Pfaue, H. (2003). Analysis of water in food by near infrared spectroscopy. *Food Chemistry*, *82*(1), 107–115. Doi: 10.1016/S0308-8146(02)00583-6.

Chen, F. L., Wei, Y. M., Zhang, B., & Ojokoh, A. O. (2010). System parameters and product properties response of soybean protein extruded at wide moisture range. *Journal of Food Engineering, 96*(2), 208–213. https://doi.org/10.1016/J.JFOODENG.2009.07.014

Chen, Q., Zhang, J., Liu, H., Li, T., & Wang, Q. (2023). Mechanism of high-moisture extruded protein fibrous structure formation based on the interactions among pea protein, amylopectin, and stearic acid. *Food Hydrocolloids, 136*, Article 108254. https://doi.org/10.1016/J.FOODHYD.2022.108254

Cornet, S. H. V., Snel, S. J. E., Schreuders, F. K. G., van der Sman, R. G. M., Beyrer, M., & van der Goot, A. J. (2022). Thermo-mechanical processing of plant proteins using shear cell and high-moisture extrusion cooking. *Critical Reviews in Food Science and Nutrition, 62*(12), 3264–3280. https://doi.org/10.1080/10408398.2020.1864618

De Angelis, D., Opaluwa, C., Pasqualone, A., Karbstein, H. P., & Summo, C. (2023). Rheological properties of dry-fractionated mung bean protein and structural, textural, and rheological evaluation of meat analogues produced by high-moisture extrusion cooking. *Current Research in Food Science, 7*, Article 100552. https://doi.org/10.1016/J.CRFS.2023.100552

Dodds, S. A., & Heath, W. P. (2005). Construction of an online reduced-spectrum NIR calibration model from full-spectrum data. *Chemometrics and Intelligent Laboratory Systems, 76*(1), 37–43. https://doi.org/10.1016/J.CHEMOLAB.2004.09.002

Duque-Estrada, P., Kyriakopoulou, K., de Groot, W., van der Goot, A. J., & Berton-Carabin, C. C. (2020). Oxidative stability of soy proteins: From ground soybeans to structured products. *Food Chemistry, 318*, Article 126499. https://doi.org/10.1016/J.FOODCHEM.2020.126499

Ellekjaer, M. R., & Isaksson, T. (1992). Assessment of maximum cooking temperatures in previously heat treated beef. Part 1: Near infrared spectroscopy. *Journal of the Science of Food and Agriculture, 59*(3), 335–343. https://doi.org/10.1002/JSFA.2740590310

Ellwanger, F., Pernice, L., Karbstein, H. P., & Emin, M. A. (2023). Investigating local residence time and thermomechanical stress profile in twin-screw extrusion of plant proteins by using the moving particle semi-implicit simulation method. *Journal of Food Engineering, 359*, Article 111665. https://doi.org/10.1016/J.JFOODENG.2023.111665

Emin, M. A. (2022). Key technological advances of extrusion processing. In P. Juliano, K. Knoerzer, J. Sellahewa, M. H. Nguyen, & R. Buckow (Eds.), *Food Engineering Innovations Across the Food Supply Chain* (pp. 131–148). Academic Press. https://doi.org/10.1016/B978-0-12-821292-9.00005-4.

Evans, A. J., Huang, S., Osborne, B. C., Kotwal, Z., & Wesley, U. (1999). Near infrared on-line measurement of degree of cook in extrusion processing of wheat flour. *Journal of Near Infrared Spectroscopy, 7*(2), 77–84. https://doi.org/10.1255/jnirs.237

Grabowska, K. J., Zhu, S., Dekkers, B. L., De Ruijter, N. C. A., Gieteling, J., & van der Goot, A. J. (2016). Shear-induced structuring as a tool to make anisotropic materials using soy protein concentrate. *Journal of Food Engineering, 188*, 77–86. https://doi.org/10.1016/j.jfoodeng.2016.05.010

Guy, R. C. E., Osborne, B. G., & Robert, P. (1996). The application of near infrared reflectance spectroscopy to measure the degree of processing in extrusion cooking processes. *Journal of Food Engineering, 27*(3), 241–258. https://doi.org/10.1016/0260-8774(95)00006-2

Högg, E., & Rauh, C. (2023). Towards a Better Understanding of Texturization during High-Moisture Extrusion (HME)—Part I: Modeling the Texturability of Plant-Based Proteins. *Foods, 12*(10). https://doi.org/10.3390/foods12101955

Jaspe, J., & Hagen, S. J. (2006). Do protein molecules unfold in a simple shear flow? *Biophysical Journal, 91*(9), 3415–3424. https://doi.org/10.1529/biophysj.106.089367

Ju, Q., Yuan, Y., Wu, C., Hu, Y., Zhou, S., & Luan, G. (2023). Heat-induced aggregation of subunits/polypeptides of soybean protein: Structural and physicochemical properties. *Food Chemistry, 405*, Article 134774. https://doi.org/10.1016/J.FOODCHEM.2022.134774

Liu, K. S., & Hsieh, F. H. (2007). Protein-Protein Interactions in High Moisture-Extruded Meat Analogs and Heat-Induced Soy Protein Gels. *Journal of the American Oil Chemists' Society, 84*(8), 741–748. https://doi.org/10.1007/S11746-007-1095-8

Mateen, A., Mathpati, M., & Singh, G. (2023). A study on high moisture extrusion for making whole cut meat analogue: Characterization of system, process and product parameters. *Innovative Food Science & Emerging Technologies, 85*, Article 103315. https://doi.org/10.1016/J.IFSET.2023.103315

Maung, T. T., Gu, B. Y., & Ryu, G. H. (2021). Influence of extrusion process parameters on specific mechanical energy and physical properties of high-moisture meat analog. *International Journal of Food Engineering, 17*(2), 149–157. https://doi.org/10.1515/ijfe-2020-0042

Meng, A., Chen, F., Zhao, D., Wei, Y., & Zhang, B. (2022). Identifying changes in soybean protein properties during high-moisture extrusion processing using dead-stop operation. *Food Chemistry, 395*, Article 133599. https://doi.org/10.1016/J.FOODCHEM.2022.133599

Nasrollahzadeh, F., Roman, L., Swaraj, V. J. S., Ragavan, K. V., Vidal, N. P., Dutcher, J. R., & Martinez, M. M. (2022). Hemp (Cannabis sativa L.) protein concentrates from wet and dry industrial fractionation: Molecular properties, nutritional composition, and anisotropic structuring. *Food Hydrocolloids, 131*, Article 107755. https://doi.org/10.1016/J.FOODHYD.2022.107755

O'Farrell, M., Bakke, K. A. H., Tschudi, J., & Wold, J. P. (2011). Near-infrared (NIR) interactance system for non-contact monitoring of the temperature profile of baked liver pâté. *Applied Spectroscopy, 65*(12), 1372–1379. https://doi.org/10.1366/11-06277

Opaluwa, C., Lott, T., Karbstein, H. P., & Emin, M. A. (2023). Encapsulation of oil in the high moisture extrusion of wheat gluten: Interrelation between process parameters, matrix viscosity and oil droplet size. *Future Foods, 7*, Article 100222. https://doi.org/10.1016/J.FUFO.2023.100222

Osen, R., Toelstede, S., Eisner, P., & Schweiggert-Weisz, U. (2015). Effect of high moisture extrusion cooking on protein–protein interactions of pea (Pisum sativum L.) protein isolates. *International Journal of Food Science & Technology, 50*(6), 1390–1396. https://doi.org/10.1111/IJFS.12783

Ozaki, Y., & Morisawa, Y. (2020). Principles and Characteristics of NIR Spectroscopy. In Y. Ozaki, C. Huck, S. Tsuchikawa, & S. B. Engelsen (Eds.), *Near-Infrared Spectroscopy* ((1st ed.,, pp. 11–35). Singapore: Springer. https://doi.org/10.1007/978-981-15-8648-4_2.

Pietsch, V. L., Bühler, J. M., Karbstein, H. P., & Emin, M. A. (2019). High moisture extrusion of soy protein concentrate: Influence of thermomechanical treatment on protein-protein interactions and rheological properties. *Journal of Food Engineering, 251*, 11–18. https://doi.org/10.1016/j.jfoodeng.2019.01.001

Pietsch, V. L., Schöffel, F., Rädle, M., Karbstein, H. P., & Emin, M. A. (2019). High moisture extrusion of wheat gluten: Modeling of the polymerization behavior in the screw section of the extrusion process. *Journal of Food Engineering, 246*, 67–74. https://doi.org/10.1016/j.jfoodeng.2018.10.031

Pietsch, V. L., Werner, R., Karbstein, H. P., & Emin, M. A. (2019). High moisture extrusion of wheat gluten: Relationship between process parameters, protein polymerization, and final product characteristics. *Journal of Food Engineering, 259*, 3–11. https://doi.org/10.1016/j.jfoodeng.2019.04.006

Pommet, M., Morel, M. H., Redl, A., & Guilbert, S. (2004). Aggregation and degradation of plasticized wheat gluten during thermo-mechanical treatments, as monitored by rheological and biochemical changes. *Polymer, 45*(20), 6853–6860. https://doi.org/10.1016/J.POLYMER.2004.07.076

Puski, G., & Konwinski, A. H. (1976). *Process of making a soy-based meat substitute*. (U.S. Patent No. 3,950,564). Washington, DC: U.S. Patent and Trademark Office.

Quevedo, M., Kulozik, U., Karbstein, H. P., & Emin, M. A. (2020). Kinetics of denaturation and aggregation of highly concentrated β-Lactoglobulin under defined thermomechanical treatment. *Journal of Food Engineering, 274*, Article 109825. https://doi.org/10.1016/J.JFOODENG.2019.109825

Riazi, F., Tehrani, M. M., Lammers, V., Heinz, V., & Savadkoohi, S. (2023). Unexpected morphological modifications in high moisture extruded pea-flaxseed proteins: Part I, topological and conformational characteristics, textural attributes, and viscoelastic phenomena. *Food Hydrocolloids, 136*, Article 108304. https://doi.org/10.1016/J.FOODHYD.2022.108304

Savitzky, A., & Golay, M. J. E. (1964). Smoothing and Differentiation of Data by Simplified Least Squares Procedures. *Analytical Chemistry, 36*(8), 1627–1639. https://doi.org/10.1021/ac60214a047

Schmid, E. M., Farahnaky, A., Adhikari, B., & Torley, P. J. (2022). High moisture extrusion cooking of meat analogs: A review of mechanisms of protein texturization. *Comprehensive Reviews in Food Science and Food Safety, 21*(6), 4573–4609. https://doi.org/10.1111/1541-4337.13030

Schreuders, F. K. G., Schlangen, M., Kyriakopoulou, K., Boom, R. M., & van der Goot, A. J. (2021). Texture methods for evaluating meat and meat analogue structures: A review. *Food Control, 127*, Article 108103. https://doi.org/10.1016/j.foodcont.2021.108103

Sharma, L. G., & Pandey, L. M. (2021). Thermomechanical process induces unfolding and fibrillation of bovine serum albumin. *Food Hydrocolloids, 112*. https://doi.org/10.1016/j.foodhyd.2020.106294

Shen, F., Ying, Y., Li, B., Zheng, Y., & Hu, J. (2011). Prediction of sugars and acids in Chinese rice wine by mid-infrared spectroscopy. *Food Research International, 44*(5), 1521–1527. https://doi.org/10.1016/J.FOODRES.2011.03.058

Shrestha, S., van 't Hag, L., Haritos, V., & Dhital, S. (2024). Fate of pulse globulin proteins molecular Structure and composition on high moisture extrusion. *Food Hydrocolloids*, *149*, 109512. Doi: 10.1016/J.FOODHYD.2023.109512.

Skåra, T., Stormo, S. K., Skipnes, D., Kondjoyan, A., Sivertsen, A., Gins, G., van Derlinden, E., Valdramidis, V. P., & van Impe, J. F. M. (2014). Estimation of surface temperature and thermal load in short-time heat treatment of surimi through reflectance spectroscopy and heat transfer modeling. *Journal of Food Engineering, 120*(1), 75–80. https://doi.org/10.1016/J.JFOODENG.2013.07.022

Sun, D., Wu, M., Zhou, C., & Wang, B. (2022). Transformation of high moisture extrusion on pea protein isolate in melting zone during: From the aspects of the rheological property, physicochemical attributes and modification mechanism. *Food Hydrocolloids, 133*, Article 108016. https://doi.org/10.1016/J.FOODHYD.2022.108016

Taghian Dinani, S., Charles Carrillo, M. F., Boom, R., & van der Goot, A. J. (2023). Quality improvement of plant-based meat alternatives by addition of iota carrageenan to pea protein–wheat gluten blend. *European Food Research and Technology, 249*, 1637–1654. https://doi.org/10.1007/s00217-023-04244-7

Tian, T., Ren, K., Cao, X., Peng, X., Zheng, L., Dai, S., Tong, X., Zeng, Q., Qiu, S., Wang, H., & Jiang, L. (2023). High moisture extrusion of soybean-wheat co-precipitation protein: Mechanism of fibrosis based on different extrusion energy regulation. *Food Hydrocolloids, 144*, Article 108950. https://doi.org/10.1016/J.FOODHYD.2023.108950

Uddin, M., Ishizaki, S., Okazaki, E., & Tanaka, M. (2002). Near-infrared reflectance spectroscopy for determining end-point temperature of heated fish and shellfish meats. *Journal of the Science of Food and Agriculture, 82*(3), 286–292. https://doi.org/10.1002/JSFA.1032

Uddin, M., Okazaki, E., Ahmad, M. U., Fukuda, Y., & Tanaka, M. (2005). Noninvasive NIR spectroscopy to verify endpoint temperature of kamaboko gel. *LWT - Food Science and Technology, 38*(8), 809–814. https://doi.org/10.1016/j.lwt.2004.10.008

Uddin, M., Okazaki, E., Ahmad, M. U., Fukuda, Y., & Tanaka, M. (2006). NIR spectroscopy: A non-destructive fast technique to verify heat treatment of fish-meat gel. *Food Control, 17*(8), 660–664. https://doi.org/10.1016/j.foodcont.2005.04.009

van der Sman, R. G. M., & van der Goot, A. J. (2023). Hypotheses concerning structuring of extruded meat analogs. *Current Research in Food Science, 6*, Article 100510. https://doi.org/10.1016/j.crfs.2023.100510

van Staveren, D. (2020, February 24). *Benefits of NIR spectroscopy: Part 2*. https://www.metrohm.com/en_nl/discover/blog/20-21/benefits-of-nir-spectroscopy–part-2.html.

Wehrmaker, A. M., Zenker, H. E., de Groot, W., Sanders, M., van der Goot, A. J., Janssen, A. E. M., Keppler, J., & Bosch, G. (2022). Amino Acid Modifications During the Production (Shearing, Sterilization) of Plant-Based Meat Analogues: An Explorative Study Using Pet Food Production as an Example. *ACS Food Science & Technology, 2*(11), 1753–1765.

Wittek, P., Ellwanger, F., Karbstein, H. P., & Emin, M. A. (2021). Morphology development and flow characteristics during high moisture extrusion of a plant-based meat analogue. *Foods, 10*(8), 1753. https://doi.org/10.3390/foods10081753

Wittek, P., Zeiler, N., Karbstein, H. P., & Emin, M. A. (2021). High moisture extrusion of soy protein: Investigations on the formation of anisotropic product structure. *Foods, 10*(1), 102. https://doi.org/10.3390/foods10010102

Wold, J. P. (2016). On-line and non-destructive measurement of core temperature in heat treated fish cakes by NIR hyperspectral imaging. *Innovative Food Science and Emerging Technologies, 33*, 431–437. https://doi.org/10.1016/j.ifset.2015.12.012

Wold, J. P., O'Farrell, M., Tschudi, J., Eskildsen, C. E., Andersen, P. V., & Ottestad, S. (2020). In-line and non-destructive monitoring of core temperature in sausages during industrial heat treatment by NIR interaction spectroscopy. *Journal of Food Engineering, 277*, Article 109921. https://doi.org/10.1016/j.jfoodeng.2020.109921

Wold, S., Sjöström, M., & Eriksson, L. (2001). PLS-regression: A basic tool of chemometrics. *Chemometrics and Intelligent Laboratory Systems, 58*(2), 109–130. https://doi.org/10.1016/S0169-7439(01)00155-1

Wolz, M., & Kulozik, U. (2015). Thermal denaturation kinetics of whey proteins at high protein concentrations. *International Dairy Journal, 49*, 95–101.

Zhang, J., Guo, C., Cui, X., Cai, W., & Shao, X. (2019). A two-level strategy for standardization of near infrared spectra by multi-level simultaneous component analysis. *Analytica Chimica Acta, 1050*, 25–31. https://doi.org/10.1016/J.ACA.2018.11.013

Zhang, X., Zhao, Y., Zhang, T., Zhang, Y., Jiang, L., & Sui, X. (2022). High moisture extrusion of soy protein and wheat gluten blend: An underlying mechanism for the formation of fibrous structures. *LWT, 163*, Article 113561. https://doi.org/10.1016/J.LWT.2022.113561

Zhang, Z., Zhang, L., He, S., Li, X., Jin, R., Liu, Q., Chen, S., & Sun, H. (2022). High-moisture extrusion technology application in the processing of textured plant protein meat analogues: A review. *Food Reviews International*. https://doi.org/10.1080/87559129.2021.2024223